ELSEVIER

Journal of Volcanology and Geothermal Research 100 (2000) 395–412

Journal of volcanology and geothermal research

www.elsevier.nl/locate/jvolgeores

Pyroclastic current dynamic pressure from aerodynamics of tree or pole blow-down

A.B. Clarke*, B. Voight

Penn State University, Department of Geosciences, University Park, PA, USA

Abstract

The common occurrence of tree and pole blow-down from pyroclastic currents provides an opportunity to estimate properties of the currents. Blow-down may occur by uprooting (root zone rupture), or flexure or shear at some point on the object. If trees are delimbed before blow-down, each tree or pole can be simulated by a cylinder perpendicular to the current. The force acting on a cylinder is a function of flow dynamic pressure, cylinder geometry, and drag coefficient. Treated as a cantilever of circular cross-section, the strength for the appropriate failure mode (rupture, uprooting or flexure) can then be used to estimate the minimum necessary current dynamic pressure. In some cases, larger or stronger standing objects can provide upper bounds on the dynamic pressure. This analysis was treated in two ways: (1) assuming that the current properties are vertically constant; and (2) allowing current velocity and density to vary vertically according to established models for turbulent boundary layers and stratified flow. The two methods produced similar results for dynamic pressure. The second, along with a method to approximate average whole-current density, offers a means to estimate average velocity and density over the height of the failed objects. The method is applied to several example cases, including Unzen, Mount St. Helens, Lamington, and Merapi volcanoes. Our results compare reasonably well with independent estimates. For several cases, we found that it is possible to use the dynamic pressure equations developed for vertically uniform flow, along with the average cloud density multiplied by a factor of 2–5, to determine average velocity over the height of the failed object.

Keywords: pyroclastic current; dynamic pressure; tree or pole blow-down

1. Introduction

Valentine (1998) recently analyzed damage to structures caused by volcanic blasts and surges by means of analogy to the effects of nuclear weapons (Glasstone and Dolan, 1977). The study classified the range of current dynamic pressure based on the level of damage incurred. Some others, such as Hool (1958), Asahi et al., (1992), and Clarke et al. (1997) have used damage to poles, trees and structures and movement of objects to estimate dynamic pressure and equivalent wind velocity of dilute pyroclastic currents. Because damage of this sort is common, a more rigorous quantitative treatment may be useful in determining current properties. In order to simplify the complex processes, we have chosen to focus on simple cylindrical geometries and to model the near-surface velocity and density variations with well-established relationships for turbulent boundary layers and pyroclastic currents.

The following procedure is proposed for reconstructing the properties of pyroclastic currents: (1)

* Corresponding author. Tel.: + 1-814-863-3965; fax: + 1-814-863-7823.

E-mail address: aclarke@geosc.psu.edu (A.B. Clarke).

0377-0273/00/$ - see front matter
PII: S0377-0273(00)00148-7

Table 1
Notation

Symbol	Definition	Defining equation	Units
a	Constant of logarithmic decay of deposit thickness	(10)	L^{-1}
A	Frontal area ($A = 2rh$ for cylinders)		L^2
b	Constant of logarithmic decay of deposit thickness	(11)	
C_{avg}	Maximum average particle volume concentration in pyroclastic current	(13)	
C_D	Coefficient of drag		
C_{ho}	Average particle volume concentration over height of object		
C_i	Particle volume concentration at reference height $h/h_c = 0.01$		
D	Drag force	(1)	MLT^{-2}
dD	Differential drag force over h to $h + dh$	(5)	MLT^{-2}
E	Void ratio		
h	Height above point of failure on object		L
h_c	Total height of current		L
h_f	Height of failure on object		L
h_o	Height of failed object		L
I, I_h	Area moment of inertia of cross-section of failed object	(21), (27)	L^4
k	von Karman constant ($k = 0.4$)		
K	Height of surface roughness		L
M	Applied moment	(4), (5)	ML^2T^{-2}
M_{ult}	Failure/ultimate bending moment	(7), (23b), (26)	ML^2T^{-2}
M_{yield}	Yield bending moment	(7), (23b)	ML^2T^{-2}
P_{dyn}	Dynamic pressure	(2), (8), (22)	$ML^{-1}T^{-2}$
N_R	Distribution Rouse number	(16)	
Re	Reynolds number	(3)	
R	Distance downstream from arbitrary reference point		L
R_f	Distance from arbitrary reference point to failed object	See Fig. 1	L
R_o	Distance from arbitrary reference point to end of current deposit	See Fig. 1	L
r	Failed object radius		L
r_i	Inner radius of hollow object		L
r_l	Tree limb extent from tree trunk		L
r_o	Outer radius of hollow object		L
t	Deposit thickness	(9)	L
t_f	Deposit thickness at failed object		L
t_o	Deposit thickness at end of deposit		L
U^*	Shear velocity	(20), (25)	LT^{-1}
V	Current velocity	(19)	LT^{-1}
V_{ho}	Average current velocity over h_o		LT^{-1}
Vol	DRE volume (per unit width of sediment) in current to pass failed object	(12)	L^2
w_i	Settling velocity of particles of class size i		LT^{-1}
ϕ	Log_{-2} of particle size in mm		
μ	Bulk current viscosity		$ML^{-1}T^{-1}$
μ_v	Suspending vapor viscosity		$ML^{-1}T^{-1}$
ρ	Bulk current density	(15)	ML^{-3}
ρ_{avg}	Maximum average bulk current density over full height of current	(14), (17)	ML^{-3}
ρ_{ho}	Average bulk current density over height of failed object		ML^{-3}
ρ_s	Solid particle density		ML^{-3}
ρ_v	Suspending vapor density		ML^{-3}
σ	Maximum applied stress		$ML^{-1}T^{-2}$
$\sigma_{ult,yield}$	Failure, yield strength of object		$ML^{-1}T^{-2}$
τ_o	Wall shear stress		$ML^{-1}T^{-2}$

establish dynamic pressure–force relationships for objects enclosed in a pyroclastic current; (2) develop an equation for dynamic pressure of the current in terms of breaking strength and object dimensions; and (3) estimate velocity and density profiles for the current. In this paper, these procedures are applied to example cases for comparison with independent estimates of the key parameters. Cylindrical objects are examined, but in principle the same approach can be used for objects of different shape and drag coefficient. The necessary equations are developed (notation as in Table 1), and equations are applied to selected cases as summarized in Table 1.

2. Dynamic pressure–force relationships

First we determine the force applied to a cylindrical pole by a pyroclastic current, assuming the axis of the pole is perpendicular to the current and the properties of the current are constant over the height of the pole. The force of aerodynamic drag, D, over any body is given by:

$$D = \tfrac{1}{2}\rho V^2 A C_D \tag{1}$$

where D is drag force, ρ is density of the current, V is velocity of the current, A is the frontal area of the object ($A = 2rh$ for a cylinder), and C_D is the coefficient of aerodynamic drag. Dynamic pressure is:

$$P_{\text{dyn}} = \tfrac{1}{2}\rho V^2 \tag{2}$$

$C_D \cong 1.1$ for $10 < Re < \sim 4 \times 10^5$ (Rae and Pope, 1984; Anderson, 1991; Panton, 1996), where:

$$Re = \frac{2rV\rho}{\mu} \tag{3}$$

where Re is Reynolds number and μ is the bulk viscosity of the flow (Panton, 1996; Anderson, 1991). Therefore we generally assume $C_D = 1.1$ and address the validity of this assumption later in the text.

3. Bending moment and ultimate, yield strengths

Next we relate Eq. (1) to the material properties of the cylinder in order to determine the dynamic pressure that is required to cause the observed damage. The bending moment M on a cylinder is:

$$M = P_{\text{dyn}} C_D r h^2, \tag{4}$$

assuming that the velocity and density of the flow are constant with height, where h is the height of the object above the plane of breakage. For the general case, allowing density and velocity to vary vertically, we have:

$$M = \int_{h_f}^{h_o} h \, \mathrm{d}D = 2rC_D \int_{h_f}^{h_o} h P_{\text{dyn}} \, \mathrm{d}h, \tag{5}$$

where $\mathrm{d}D = 2rC_D P_{\text{dyn}} \, \mathrm{d}h$ and is the differential drag of the cross-sectional element between h and $h + \mathrm{d}h$, h_f is the height of the point of failure and h_o is the total height of the failed object. Vertical variations of the current density and velocity are discussed later in the text. The resulting maximum stress σ in the cylinder at the height of failure is:

$$\sigma = \frac{Mr}{I} \tag{6}$$

(Beer and Johnston, 1981), where I is the area moment of inertia of the horizontal cross-section. The bending moment at failure, M_{ult}, and the moment at yield, M_{yield}, for a cylinder of outer radius r are:

$$M_{\text{ult,yield}} = \frac{I\sigma_{\text{ult,yield}}}{r} \tag{7}$$

where σ_{ult} is the ultimate failure strength of the material and σ_{yield} is the yield strength.

Combining Eqs. (4) and (7) and rearranging gives the dynamic pressure (Clarke et al., 1997) at failure or yield:

$$P_{\text{dyn}} = \frac{M_{\text{ult,yield}}}{rh^2 C_D} \tag{8a}$$

$$P_{\text{dyn}} = \frac{I\sigma_{\text{ult,yield}}}{r^2 h^2 C_D} \tag{8b}$$

Eqs. (8a) and (8b) assume that current properties are *vertically uniform*. Eq. (5) will be integrated later for *vertically non-uniform* current assumptions.

4. Density estimates for pyroclastic current

4.1. Average current bulk density

Assuming that the natural log (cm) of current

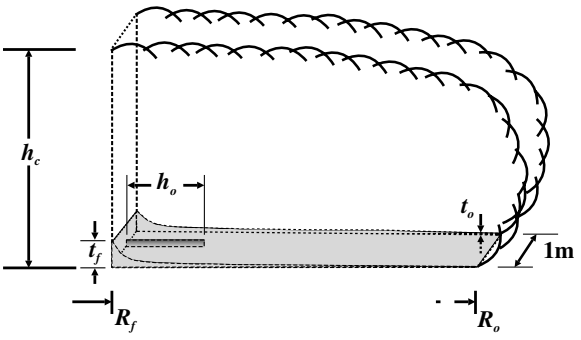

Fig. 1. Dimensions used for whole-current average density estimates of Section 4. The schematic is not to scale and shows a profile of an inflated current, a deposit of logarithmically decaying thickness, a failed cylindrical object, and all relevant parameters. Dimensions are: current height, h_c: failed object height, h_o; deposit thickness at failure site, t_f; deposit thickness at distal end of current deposit, t_o; distance downstream of failed object from arbitrary reference point, R_f; distance downstream of end of deposit from arbitrary reference point, R_o.

deposit thickness varies with distance in meters downstream from an arbitrary reference point (Wohletz and Sheridan, 1979; Wohletz, 1998), we can estimate the thickness of the deposit at any point as:

$$t = e^{(aR+b)} \tag{9}$$

where a and b are constants and R is the distance downstream from the reference point. Using two known points and solving for a and b:

$$a = \frac{\ln t_o - \ln t_f}{R_o - R_f} \tag{10}$$

$$b = \ln t_f - R_f a \tag{11}$$

where t_f (cm) is the thickness of the deposit at the site of tree or pole failure, R_f (m) is the distance from the reference point to the location of failure, t_o (cm) is the thickness of the deposit at R_o and R_o (m) is the distance from the reference point to the end of the current deposit. In our examples we assumed that $0.1 \leq t_o \leq 1.0$ cm $(-3 \leq \ln t_o \leq 0)$, allowing for some uncertainty in the end deposit thickness or location.

We use the term void ratio, E, the volumetric ratio of voids to solids (Terzaghi and Peck, 1948). Generally, we assume $E = 0.7$, as measured in pyroclastic surge deposits at Mt. Unzen, equivalent to typical void ratios for loose sand, for all of the following cases (Yamada and Yajima, 1992; Terzaghi and Peck, 1948).

By integrating the thickness of deposit from the site of failure to the end of the deposit, and multiplying by E, we estimate the total "dense rock equivalent" (DRE) volume of material to pass the broken object per meter width of current as:

$$\mathrm{Vol} = E \int_{R_f}^{R_o} e^{(aR+b)}\, dR = E \frac{1}{a}(t_o - t_f) \tag{12}$$

If we assume that the profile of the nose of the current is rectangular, we can divide by the total height of the leading part of the current h_c (not the height of the co-ignimbrite cloud) and the distance between the failure site and the end of the current deposit to derive:

$$C_{avg} = \frac{E}{100 h_c} \frac{(t_o - t_f)}{(\ln t_o - \ln t_f)} \tag{13}$$

which represents a maximum average volumetric proportion of solids per meter width of current that passes the failed object's location. The factor of 100 in the denominator is necessary for the conversion of units. Note that C_{avg} is not dependent upon distances R_o and R_f. Fig. 1 illustrates the parameters.

The corresponding maximum average current bulk density ρ_{avg} is:

$$\rho_{avg} = C_{avg}\rho_s + (1 - C_{avg})\rho_v \tag{14}$$

where ρ_s is the average density of the suspended solid particles and ρ_v is the average density of the suspending vapor.

Here we assume that all the material deposited between the failed object and the end of the deposit was suspended in the current, over this horizontal distance, during a single instant. Therefore, densities determined using this method are maxima, and the corresponding velocities are minima. We also acknowledge that downstream of the failed object, elutriation by co-ignimbrite clouds may have removed a significant proportion of fine suspended material from the region, contributing to an underestimate of maximum average concentration, C_{avg}, and of maximum average current bulk density, ρ_{avg}.

4.2. Vertical density variations

Although ρ_{avg} is the maximum average for the

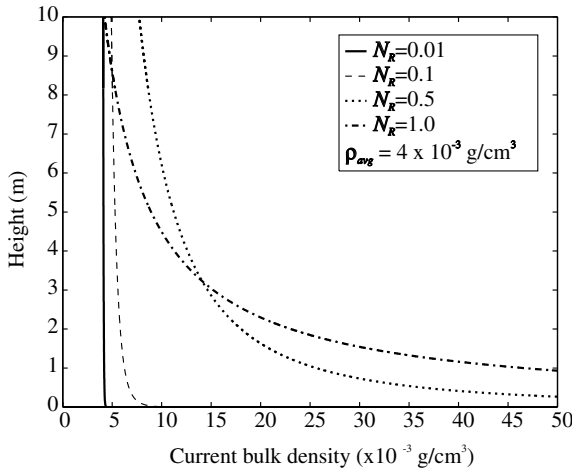

Fig. 2. Vertical density profiles for current bulk density $\rho_{avg} = 4.0 \times 10^{-3}$ g/cm^3, cloud height $h_c = 100$ m, and a variety of Rouse numbers, N_R. Note that the profiles over the bottom 10 m of current approach *vertically uniform* as N_R approaches zero.

whole-current volume, it does not represent the maximum possible density at all vertical locations in the surge, given Valentine's (1987) density profiles. A variation of his density relationship as a function of h is:

$$\rho = \rho_s C_o \left(0.0101\left(\frac{h_c}{h} - 1\right)\right)^{N_R} \quad (15)$$

where ρ_s is the solid particle density, C_o is the cloud particle volume concentration at a reference height of $h/h_c = 0.01$ and N_R is the distribution Rouse number (Valentine, 1987), a measure of a current's ability to suspend particles:

$$N_R = \frac{1}{C_{avg}} \sum_i C_i \frac{w_i}{kU^*} \quad (16)$$

where w_i is the particle settling velocity, C_i is the average volume concentration of particles in settling velocity class w_i, U^* is shear velocity which is treated later in the text, and k is the von Karman constant, where 0.4 is commonly used for surges (Valentine, 1987).

Current bulk density ρ_{avg} is related to Eq. (15) for a current of height h_c by:

$$\rho_{avg} = \rho_s C_o \left[\frac{\sum_{i=1-10h_c} \left(0.0101\left(\frac{h_c}{h_i} - 1\right)\right)^{N_R}}{10h_c}\right] \quad (17)$$

where h_i is height above the surface, increasing at intervals of 0.1 m. This equation expresses the average cloud density as a sum of densities of 0.1 m-thick, horizontal 'slices' of the cloud, divided by the number of slices, $10h_c$.

Solving for C_o, we get:

$$C_o = \frac{(10h_c\rho_{avg})}{\rho_s\left[\sum_{i=1-10h_c} \left(0.0101\left(\frac{h_c}{h_i} - 1\right)\right)^{N_R}\right]} \quad (18)$$

Fig. 2 (after Valentine, 1987) shows how density profile from Eq. (15) varies with N_R for an arbitrary $\rho_{avg} = 4.0 \times 10^{-3}$ g/cm^3 and $h_c = 100$ m. Current bulk density approaches *vertically uniform* over the bottom 10 m of current as N_R approaches zero.

5. Velocity estimates

Now we model the vertical velocity variation of the current. According to the empirical von Karman universal velocity profile law of a turbulent boundary layer over any rough surface:

$$V = U^*\left[8.48 + 5.75 \log\left(\frac{h}{K}\right)\right] \quad (19)$$

where K is the size of the roughness elements on the surface (Allen, 1970, p. 39) and U^* is the shear velocity:

$$U^* = \sqrt{\frac{\tau_o}{\rho}} \quad (20)$$

where τ_o is the wall shear stress (Allen, 1970).

We have thus far derived equations for minimum dynamic pressure P_{dyn} necessary to cause tree or pole rupture, uprooting, or bending for two separate sets of assumptions. The first set assumes *vertically uniform* current properties (Eqs. (8a) and (8b)). The second set, *vertically non-uniform* properties, assumes that density varies vertically according to a relationship developed by Valentine (1987) (Eq. (15)) and that velocity varies vertically according to von Karman's

turbulent boundary layer profile (Eq. (19)). In the following sections, we determine the dynamic pressure necessary to cause failure for several example cases. We use both sets of assumptions and compare results in order to determine the significance of vertical density and velocity variations in estimating the dynamic pressure necessary to cause observed damage. The second set of assumptions requires an iterative solution, which will be fully developed in the first example case. The second set of assumptions also provides a way to constrain average velocity and density of the current over the height of the failed object.

6. Examples

6.1. Unzen ash-cloud surge

A violent ash-cloud surge associated with the 3 June 1991 pyroclastic flow at Unzen volcano devastated the region of Kita-kamikoba, approximately 3.5 km downstream of the Fugen-dake dome. Trees and utility poles were downed, houses were burned and 43 people were killed (Yamamoto et al., 1993).

6.1.1. Vertically uniform current assumption—ruptured utility pole

Numerous utility poles ($h = 10$ m; $r = 15$ cm) were broken near their bases during the 3 June ash-cloud surge event. The area moment of inertia, I, for a solid uniform pole is:

$$I = \tfrac{1}{4}\pi r^4 \tag{21}$$

Substituting Eq. (21) into Eq. (8b), the dynamic pressure of the surge must have equaled or exceeded the following at some instant:

$$P_{\mathrm{dyn}} = \frac{1}{4}\frac{\pi r^2 \sigma_{\mathrm{ult}}}{C_D h_o^2} \tag{22}$$

Taking the nominal ultimate strength σ_{ult} in tension of Douglas Fir as 50 MPa (Beer and Johnston, 1981) and $C_D = 1.1$ with Eq. (22) results in an equivalent uniform dynamic pressure of 8.0 kPa.

6.1.2. Vertically non-uniform current—ruptured utility pole

We now repeat the calculation for a vertically non-uniform current in order to examine the significance of vertical density and velocity variations. Here we assume that the entire pole is encompassed by the turbulent boundary layer of the surge, given that most currents are fully developed within a few km downstream of their initiation point (Allen, 1970; Sparks et al., 1978). Rearranging Eq. (5) we find the expression:

$$\frac{M_{\mathrm{ult,yield}}}{2rC_D} = \int_{h_f}^{h_o} hP_{\mathrm{dyn}}\,\mathrm{d}h \tag{23}$$

We substitute Eqs. (15) and (19) into Eq. (2) to obtain an expression for P_{dyn}. Then substituting the resulting expression into Eq. (23) results in:

$$\int_{h_f}^{h_o} hP_{\mathrm{dyn}}\,\mathrm{d}h = \tfrac{1}{2}(U^*)^2\rho_s C_o (0.0101)^{N_R} \times\left[\int_{h_f}^{h_o} h\left(\frac{h_c}{h}-1\right)^{N_R}\left(8.48+5.75\log\left(\frac{h}{K}\right)\right)^2 \mathrm{d}h\right] \tag{24}$$

Combining Eqs. (23) and (24) and simplifying allows a solution for U^*, Eq. (25):

$$U^* = [M_{\mathrm{ult,yield}}]^{1/2}[rC_D\rho_s C_o (0.0101)^{N_R} \times\left[\int_{h_f}^{h_o} h\left(\frac{h_c}{h}-1\right)^{N_R}\left(8.48+5.75\log\left(\frac{h}{K}\right)\right)^2 \mathrm{d}h\right]^{-1/2} \tag{25}$$

In order to estimate current properties using Eq. (25), we must first estimate maximum average current density ρ_{avg} from the methods of Section 4. We then find preliminary values of C_o using Eq. (18) and U^* using Eq. (25) by assuming a value of Rouse number $N_R = 0.01$. Integrals are solved numerically using the trapezoidal rule. Then, we recalculate N_R using Eq. (16) and compare the result to the originally assumed value. The N_R values from Eq. (16) are calculated using the preliminary values of U^* (Eq. (25)) and the settling velocities for the grain-size distribution of the deposits at the failure site (for this example, we use the data of Miyabuchi, 1999). The method of Kunii and Levenspiel (1977, p. 76), as applied to dusty gases by Freundt and Bursik (1998, p. 194), is used to determine settling velocities for spherical particles (with assumed dusty gas density equal to the average bulk density over the height of the failed object as calculated from the originally assumed value of N_R). We next raise the value of N_R by 0.01 and

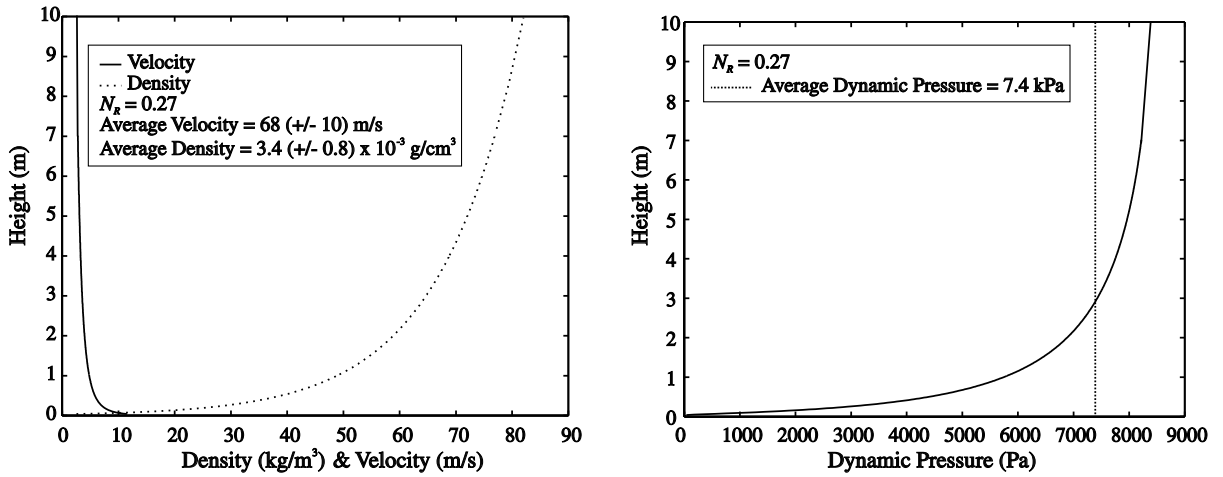

Fig. 3. Calculated current density, velocity, and dynamic pressure profiles using ruptured utility poles near Kita-kamikoba, Japan, due to the June 3, 1991 ash-cloud surge at Unzen volcano. Parameters: $h_c = 75\ m$, $\rho_{avg} = 1.9 \times 10^{-3}$ g/cm^3 ($C_{avg} = 7.3 \times 10^{-4}$), $N_R = 0.27$, $U^* = 6$ m/s.

repeat the procedure until the two values of N_R converge to within 0.02. The convergent value of N_R is used to calculate the final values of C_o (Eq. (18)), U^* (Eq. (25)), the density profile (Eq. (15)), the velocity profile (Eq. (19)), and the corresponding dynamic pressure profile (Eq. (2)). Finally, we average these parameters over the height of the failed object. The same procedure is used for most of the following examples, where the grain-size distribution at each site of object failure is used to determine the settling velocities, w_i, in Eq. (16). For this case and for our other examples, K was assumed to be 1 m and $\rho_s = 2.6$ g/cm^3.

The ruptured telephone poles at Unzen were damaged by a pyroclastic surge with deposits approximately 20 cm thick (Yamamoto et al., 1993; Nakada and Fujii, 1993). Using the methods of Section 4 with a 2.6 g/cm^3 particle density, a 400°C air density of 0.52×10^{-3} g/cm^3 (Incropera and De Witt, 1990), and an estimated cloud height of 75 m, the maximum average density of the surge $\rho_{avg} = 1.9(\pm 0.8) \times 10^{-3}$ g/cm^3 ($C_{avg} = 7.3 \times 10^{-4}$). Uncertainty in density values are due to a variation of ±10% in deposit thickness at the failure site, a variation of about ±20% in cloud height and a variation of 1 cm in deposit thickness at the end of the surge deposit, as discussed in Section 4.

The iteration converged at Rouse number, $N_R = 0.27$ where $C_o = 1.7 \times 10^{-3}$, producing $U^* = 5.8$ m/s, and corresponding values $V_{ho} = 68(\pm 10)$ m/s (average current velocity over the height of the pole), $\rho_{ho} = 3.4 \times 10^{-3}$ g/cm^3 ($C_{ho} = 13 \times 10^{-4}$) (average bulk density and volumetric concentration of current over the height of the pole), and $P_{dyn} = 7.4$ kPa (average dynamic pressure over the height of the pole). Uncertainty in velocity is due to variations in average mixture density estimates and cloud height estimates. From Eq. (3), we find that $Re \cong 9 \times 10^4$ for this current, which is within the range of values for which $C_D \cong 1.1$, our assumed coefficient. The methods of Wohletz (1998, p. 273–274) were used to determine mixture bulk viscosity for the current, μ, from particle concentration in a water vapor–air mixture at 400°C with viscosity $\mu_v \cong 2 \times 10^{-5}$ Pa-s (Incropera and De Witt, 1990).

The simplified method (assuming a *vertically uniform* current, Section 6.1.1) and the more complex method (modeling vertical density and velocity variations for a *vertically non-uniform current*, as in this section) produce similar values of P_{dyn}, 8.0 and 7.4 kPa, respectively. The velocity, density and dynamic pressure profiles for the complex treatment are shown in Fig. 3. Note that the resultant P_{dyn} profile is approximately uniform above $h = 2$ m.

Independent estimates of velocity for this case are not well constrained, as velocity varied substantially with gradient of ground slope, volume, and distance of

run out. Measurements of average "pyroclastic flow" speed using Doppler radar gave 26–28 m/s for similar events (Nakada and Fujii, 1993), but for unspecified locations. Theoretical energy-line calculations suggest for the June 3 event a peak velocity for the pyroclastic flow of about 60–70 m/s at a distance of ~2 km, but a higher detachment velocity for the surge of 80–100 m/s, 800 m upstream of its termination point (Yamamoto et al., 1993). This inferred velocity is dependent upon the assumption of a friction coefficient of 0.2. On balance the data suggest that the surge velocity at this site was ~60–100 m/s. This estimate is in accord with the values suggested by our damage analysis.

As an example of reversing the type of calculation to estimate cloud current density over the height of the failed object, we take the average of the independent velocity estimate of Yamamoto et al. (1993) of $V =$ 70 m/s, $P_{dyn} = 8.0$ kPa from Eq. (22), and solve Eq. (2) for ρ. This calculation suggests that the current density over the height of the pole was $\tilde{}3.3 \times 10^{-3}$ g/cm^3, reasonably close to the value $\rho_{ho} = 3.4 \times 10^{-3}$ g/cm^3 obtained by modeling the velocity and density profiles as in Sections 4 and 5.

6.1.3. Uprooted Japanese cedar

Trees of nominal size $h = 12$ m and $r = 15$ cm were uprooted by the pyroclastic surge from the June 3, 1991 event, approximately 3–3.5 km east–southeast of the dome, slightly closer to the dome than the aforementioned utility poles. Although the trunks of the trees are not cylinders of constant radius, estimates of dynamic pressure can be made using a variation of the above model. If it is assumed that the trees were delimbed before being toppled, then they may be modeled as cylinders. Noting that any remaining branches will change the C_D and frontal area of the tree. The simple calculation, using $C_D = 1.1$ yields an upper-bound P_{dyn}. Alternatively, the limbs and branches may be included as cylinders of different size and orientation, making the calculation complex.

Test data of Japanese cedar indicates that the uprooting moment M_{ult} is given by:

$$M_{ult} = 1.36 \times 10^7 r^3 \quad (26)$$

where r is the radius of the tree trunk (m) and M_{ult} is failure moment in (N-m) (Yamada and Yajima, 1992). Substituting Eq. (26) into Eq. (8a) (assuming a *vertically uniform* current) results in a $P_{dyn} = 1.9$ kPa required for uprooting to occur.

Using the same density and procedures used in Section 6.1.2 with M_{ult} estimated from Eq. (26), results in an iteration that converges at $N_R = 0.45$, where corresponding values are $U^* = 2.5$ m/s, $V_{ho} =$ 32 (± 5) m/s, $\rho_{ho} = 4.4 \times 10^{-3}$ g/cm^3 ($C_{ho} = 17 \times 10^{-4}$), and $P_{dyn} = 1.9$ kPa, the same as that determined from the simpler method. The dynamic pressure necessary to rupture the utility poles exceeds that required to uproot Japanese Cedar, making the ruptured telephone poles the dynamic pressure-limiting case.

6.2. Mount St. Helens directed blast—ruptured trees

Thousands of Douglas fir and Western hemlock trees were uprooted or ruptured by the 1980 directed blast surge from the north face of Mount St. Helens, comprising 1.6 billion board-feet by volume (Snellgrove et al., 1983). Most of the damaged trees were delimbed before or during blow-down, based on the observation that most felled trunks were limbless (Waitt, 1981; Kieffer, 1981; Moore and Sisson, 1981; Snellgrove et al., 1983). This justifies modeling them as cylinders. In most situations at Mount St. Helens the forest was toppled *en masse*, such that there was a "group effect" to the damage. In other instances, isolated trees fell, and our example is applied to such cases.

We consider a tree ($h = 15$ *m*; $r = 50$ cm) at a point approximately 8 km northeast of the source explosion. It failed just above the ground. Using $\sigma_{ult} = 50$ MPa for Douglas Fir (Beer and Johnston, 1981) and Eq. (22) (assuming a *vertically uniform* current), the dynamic pressure necessary for such damage is approximately 39.7 kPa. Next we re-estimate the properties modeling the current as *vertically non-uniform*.

Blast surge deposits in this location vary from 40 to 50 cm thick, with the average about 45 cm (Druitt, 1992; observations, 1996). At 200°C, air density is $\sim 0.74 \times 10^{-3}$ g/cm^3. The observed current-front height is 400 m (Moore and Rice, 1984). Using these values and the methods of Section 4.1, the estimated average current density 8 km from the vent is approximately 0.94 (± 0.2) $\times 10^{-3}$ g/cm^3 ($C_{avg} = 3.6 \times 10^{-4}$). Using the methods of Section 6.1.2 and

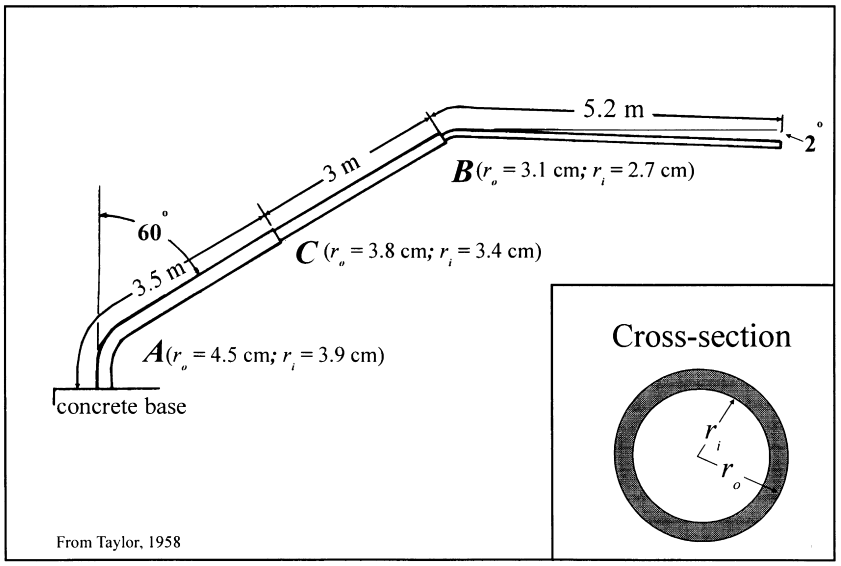

Fig. 4. Post-damage geometry of hollow flagpole at Higaturu village, Papua (after Taylor, 1958).

grain-size data of Druitt (1992), convergence occurs at $N_R = 0.61$, where $C_o = 2.7 \times 10^{-3}$, for which $U^* = 9.4$ m/s, $\rho_{ho} = 8.3 \times 10^{-3}$ g/cm^3 ($C_{ho} = 32 \times 10^{-4}$), $V_{ho} = 120(\pm 10)$ m/s, and $P_{dyn} = 43$ kPa, close to the estimate of Eq. (22) above. $Re \cong 2.3 \times 10^5$ for this current, approaching the upper limit of values valid for our assumed C_D of 1.1. Our estimated range of velocity is consistent with current velocities of 120–140 m/s estimated from timed photographs and satellite data in this region (Moore and Rice, 1984).

We now take the average observed velocity of 130 m/s of Moore and Rice (1984), assume it applies to the damaged area and use $P_{dyn} = 39.7$ kPa from Eq. (22). Eq. (2) suggests that the average surge density over the height of the trees is 4.7×10^{-3} g/cm^3 ($C_{ho} = 18 \times 10^{-4}$), about two thirds of the value obtained by the methods of Section 6.1.2.

6.3. Mount Lamington fountain-collapse surge—damage to a pole at Higaturu

In the 1951 eruption of Mount Lamington, Papua New Guinea, a step-tapered hollow metal flagpole 11 m high, at Higaturu village located 6 km north of the vent, was bent at two heights by a fountain-collapse pyroclastic surge (Taylor, 1958). At point A, near the base, the pole bent 60° from the vertical; at point B, about 5 m from the top, it bent 32° from its original position (Fig. 4). Analysis is complicated by the complexity of the deformation and the geometry of the pole.

6.3.1. Bending of hollow pole at points A and B

Because the pole bent but did not rupture, we infer that the bending moment at points A and B must have produced a stress greater than the yield stress for the steel, but less than its rupture stress. Bending moment tests were performed on the middle (C) ($r_o = 3.8$ cm; $r_i = 3.4$ *cm*) and upper (B) ($r_o = 3.1$ cm; $r_i = 2.7$ cm) sections of the flagpole (Dunning, 1958; See Fig. 4). Inner and outer radii of the hollow flagpole are given by r_i and r_o, respectively. Extrapolation of this test data was used to determine the resisting bending moment for the lower section (A) ($r_o = 4.5$ cm; $r_i = 3.9$ cm). Therefore, we use the following values of yield moment M_{yield} for our calculations: 6800 N-m at A; 1800 N-m at B; and 4300 N-m at C. The handbook value of rupture strength for typical steel is $\sigma_{ult} = 450$ MPa (Beer and Johnston, 1981; Popov, 1952). All values are for a pole at room temperature.

Eq. (8a) (where r is the average outer radius above the point in question; $r = 3.8$ cm for A) and the above yield moments of the pole show that, for a *vertically*

uniform current, the dynamic pressure necessary to initially bend the pole at A is lower than that required to initially bend it at B. An initially vertical pole could bend at A at $P_{dyn} = 1.3$ kPa, and at B at $P_{dyn} = 2.1$ kPa, indicating that point B is the dynamic pressure-limiting location. Therefore, if the pole bends at B from its original upright position, the current dynamic pressure must have reached or exceeded 2.1 kPa, in which case the pole bends at both A and B. We will next repeat the procedure for a *vertically non-uniform* current, modeling density and velocity profiles as described in Sections 4 and 5.

The surge deposits at Higaturu were between 15 and 25 cm thick, with a 20 cm average (Taylor, 1958). Using the methods of Section 4, assuming a 100 m current height, we estimate $\rho_{avg} = 1.4 (\pm 0.4) \times 10^{-3}$ g/cm^3 ($C_{avg} = 5.4 \times 10^{-4}$). We use the methods of Section 6.1.2 with our modeled vertical variations of density and velocity and $M_{yield} =$ 6800 N-m at A and $M_{yield} = 1800$ N-m at B. Convergence occurs at $N_R = 0.48$, where $C_o = 3.3 \times 10^{-3}$, resulting in $U^* = 2.8$ m/s, $\rho_{ho} = 4.3 \times 10^{-3}$ g/cm^3 ($C_{ho} = 17 \times 10^{-4}$), $V_{ho} = 33(\pm 4)$ m/s, and $P_{dyn} =$ 2.2 kPa. This is very close to the value estimated above assuming a *vertically uniform* current. For this profile, the current is just sufficient to cause bending at B, the applied moment at A is 1.6 times that necessary to cause bending, and the applied moment at point C is ~4500 N-m, which according to test data should have been sufficient to cause bending at C. It is unclear why bending never occurred at C. Possibilities will be discussed later. Next, we consider the upper-bound values, constrained by the rupture strength of the pole at A.

The area moment of inertia for hollow cylinders is:

$$I_h = \frac{1}{4}\pi(r_o^4 - r_i^4) \quad (27)$$

We first combine Eq. (27) with Eq. (7) and $\sigma_{ult} =$ 450 MPa (the handbook value for steel) to determine M_{ult}. Modeling the current as *vertically non-uniform*, as described in Section 6.1.2, shows that for rupture at *A* of an upright pole, the calculations converge at $N_R = 0.46$ where $C_o = 3.1 \times 10^{-3}$, resulting in $U^* = 3.1$ m/s, $V_{ho} = 38$ m/s, $\rho_{ho} = 4.7 \times 10^{-3}$ g/cm^3 ($C_{ho} = 18 \times 10^{-4}$), and $P_{dyn} = 2.8$ kPa.

These estimates suggest that a current with a dynamic pressure greater than 2.1 kPa could bend the upright pole at A and B simultaneously, and a current with dynamic pressure in excess of 2.8 kPa could rupture the upright pole at A, thus constraining the dynamic pressure of the current during the initial stages of damage to the pole. However, this range of values is narrow, indicating that if bending occurred as described above, for the given strength characteristics, the pole would have been very close to failure at A. This is contrary to evidence acquired by examination of the pole immediately after the damage occurred (Dunning, 1958). In the next section, we will consider an alternative scenario in which bending initiates at A and later commences at B.

Our estimate of velocity necessary to initiate bending at A and at B (33 m/s) is considerably lower than the previous calculation of 98 m/s reported in an appendix to Taylor (1958) by J.N. Hool, in which it was assumed that the current had the density of air. The difference in result emphasizes the importance of considering appropriate current densities.

6.3.2. Effects of strain-hardening and an oblique pole

The above calculations provide first-order estimates and do not account for strain hardening as the pole bends, nor for decreasing drag as the pole becomes oblique to the current direction. Below we explore the effects of these two complexities by considering two possible damage scenarios.

Test data indicate that the bending moment of pole resistance increased due to strain hardening by ~30 N-m per degree of bending at B, and by ~80 N-m per degree of bending at C (Dunning, 1958). We assume for illustration purposes that the pole at A strain hardened at the same rate as at C. We do not consider strain-induced changes in rupture strength of steel.

We first assume that bending initially occurred at A and B, more or less in unison. As calculated above in Section 6.3.1, the surge must have reached or exceeded 2.1 kPa dynamic pressure in order to bend the pole at A and B from the originally upright position, but did not exceed 2.8 kPa in order to avoid rupture at A. However, as pole deformation progresses, we consider the reduced frontal area of the pole as it becomes oblique to the direction of the current and the increased M_{yield} due to strain hardening. We account for apparent shortening by

calculating the height of the pole perpendicular to the current direction. The apparent length of each pole section is calculated by multiplying the length of each pole section by the cosine of the total deflection of the section from the vertical. For a 30° bend at A, the apparent length of the pole from A to B is the length of the pole from A to B (~6 m) multiplied by cos30°. For an additional 30° bend at B, the apparent length of the section above B is the length of pole above B (~5 m) multiplied by cos60°. We account for strain hardening using the rates stated in the previous paragraph. Because estimates of dynamic pressure are similar for the two sets of assumptions tested previously, we assume a vertically uniform current for most of the following examples in order to simplify the calculations.

Again, supposing the pole initially bends at A and B simultaneously, the pole will eventually reach a position where the bend at both A and B is 30°. For this geometry (30° bend at A; 30° bend at B) according to the strain-hardening relationships stated previously, bending will continue at A with an applied moment of ~9200 N-m and will continue at B with an applied moment of ~2700 N-m. Using these new values of M_{yield}, Eq. (8a), and apparent lengths of the pole sections, we find that $P_{\text{dyn}} = 12$ kPa is just adequate to bend the pole at B to its final position, and is over 3 times that required to continue bending at A. Referring to the final geometry of the pole (Fig. 4), the pole stopped bending at B at this stage, where 12 kPa is the maximum possible dynamic pressure of the current for this phase of deformation. But, remembering that the failure strength of the pole at A is $M_{\text{ult}} =$ 450 MPa, using Eq. (7) and Eq. (8a) for a pole of this geometry, we find that $P_{\text{dyn}} = 5.8$ kPa is sufficient to rupture the pole at A. However, $P_{\text{dyn}} = 5.8$ kPa is not sufficient to bend the pole at B to its final position if the bending initiated and progressed at A and B in unison. Therefore, we consider another possible sequence of events.

If the pole were to initially bend at A from upright (but not at B), we find that $P_{\text{dyn}} = 1.3$ kPa (Section 6.3.1) is sufficient to do so. As the pole continues to bend at ***A***, P_{dyn} required to continue bending at ***A*** increases. As the pole bends at ***A*** from 0° to 45°, the necessary dynamic pressure to cause bending at *A* increases from 1.3 to 4.2 kPa, due to strain hardening and increasing pole obliquity to the direction of the current. As the pole bends at A from 0° to 45°, the dynamic pressure just sufficient to continue bending at A is never sufficient to initiate bending at B. But, as the pole exceeds 45° from vertical at A, the dynamic pressure necessary to continue bending at A ($\geq$4.2 kPa) is also sufficient to initiate bending at B. With the pole in the 45° position, the dynamic pressure required for rupture at A is ~5.7 kPa, but this value increases as bending occurs at B. Therefore, as the pole bends beyond 45° at A, the pole could conceivably begin to bend at A and B simultaneously without rupturing at A. As the damage continues to its final state, the current dynamic pressure required for bending increases, reaching a maximum of ~24 kPa (with corresponding velocity $V_{\text{ho}} = 130$ m/s). The dynamic pressure necessary for rupture at the final position is ~30 kPa.

We therefore suggest that it is possible, given the aforementioned strength characteristics, that the pole began bending at A under the force of a current. The pressure required to cause this bending increased in time from 1.3 to 4.2 kPa. Then, upon reaching a 45° bend at A, bending could have continued bending at A and also commenced at B, with a current dynamic pressure in excess of 4.2 kPa. As the damage continued to its final state, the current dynamic pressure increased but never exceeded 24 kPa. The range of possible velocities for this event, based on the preceding damage analysis, is 29–130 m/s. This may be compared with Taylor's (1958) rough estimates of 27–93 m/s based on eyewitness accounts of timing of the event:

> "Reconstructing the actions of people who witnessed the climactic explosion roughly limited the period of time from the initial explosion to the incidence of the return wind which rolled the nuée back. This estimate suggested a possible lower limit of five minutes and an upper limit of ten minutes. Assuming that the initial vulcanian explosion lasted three minutes and taking 7 miles as the general distance covered by the nuée on the northern slopes, then the velocity was between 60 and 210 miles per hour."

A question remains as to how the pole remained undamaged at C, when calculations suggest that the range of dynamic pressure estimated above would have been sufficient to bend the pole at C. It is

possible that the temperature of the pole increased due to exposure to the surge, changing its strength characteristics; however, such a short exposure time (on the order of tens of seconds) should not have been sufficient to significantly heat the steel. It is also necessary to remember that the strength characteristics at A were estimated by extrapolation of data at the other two points, for the purposes of sample calculations. In addition, it has been suggested that welding between pole sections (at A, B & C) could have contributed to strength inconsistencies at these joints, with location B being the weakest and location C the strongest (James Ewart, personal communication).

7. Merapi Volcano ash-cloud surge

Here we apply the method to ruptured and uprooted trees on the slopes of Merapi volcano, Java, resulting from a surge associated with a large dome-collapse nuée ardente that occurred at 10:54 a.m. on 22 November 1994 (Abdurachman et al., 2000 – this volume).

7.1. Distribution of damage and deposits

7.1.1. Tree damage

On the south–southwest flank of Merapi, the surge cloud removed vegetation and toppled nearly all the trees. A narrow strip of singed vegetation surrounds the main lobes of the surge deposit. In an adjacent region the trees are uprooted, irregularly broken, or bent. Only the upper parts of trees are broken or damaged at the external limit of the affected area. This is interpreted to have been due to the buoyant rise of the distal surge cloud (Abdurachman et. al., 2000 – this volume; Kelfoun et. al., 2000 – this volume).

7.1.2. Deposits

The surge deposit near Turgo village (~6 km SSW of the summit dome) is approximately 5 cm deep (Abdurachman et al., 2000 – this volume). The components are mainly fresh, poorly vesicular, crystalline lithics derived from the 1992–1994 dome complex. Particles in the deposit are primarily sand-sized, but the deposit also contains sparse lapilli as much as 3 cm in diameter (Abdurachman et al., 2000 – this volume). Because the particles are mostly sand-sized and non-vesicular, the particle density of 2.6 g/cm^3 is used in the following calculations. From measurements of sediment mass and bulk volume, we calculated void ratios of 0.55–1.0 at Turgo; thus 0.7 is a reasonable nominal value for calculations. Grain-size analysis for this location gives $\phi_{\text{mean}} = 1.4$, with an Inman sorting of 1.4ϕ. The full grain-size distribution is used below when determining distribution Rouse number from Eq. (16) for a *vertically non-uniform* current (as in Section 6.1.2).

7.1.3. Observations of surge clouds

Observations of this event indicate that the ash cloud surge was about 130 m high in the narrows on the east side of Turgo Hill (Abdurachman et al., 2000 – this volume; Kelfoun et al., 2000 – this volume). However, observations suggest that the surge cloud expanded laterally beyond the hill and simultaneously decreased in thickness, which we estimate to be about 50 m.

7.2. Current property calculations near Turgo Village

7.2.1. Uprooted trees

The surge near Turgo (near the channel edge) uprooted trees with $h = 16$ m and $r = 20$ cm. Using test data on Japanese cedar to give uprooting moment (Eq. (26)), the minimum dynamic pressure necessary to cause the damage is 1.9 kPa (Eq. (8a)). However, because these trees retained many of their limbs, $C_D = 1.1$ may be incorrect. We therefore repeat the calculations using wind tunnel data from tests of live trees, where $C_D = 0.6$ (Allen, 1982). Although this is lower than our originally assumed value of 1.1, the branches increase the object frontal area. Eq. (23) becomes:

$$\frac{M_{\text{ult,yield}}}{2r_{\text{l}}C_D} = \int_{h_{\text{f}}}^{h_{\text{o}}} hP_{\text{dyn}}\,\mathrm{d}h \tag{23b}$$

where r_{l} is the limb extent from the trunk, which during a strong wind is approximately 60% of the ordinary extent (Allen, 1982). We estimate $r_{\text{l}} = 2$ m for the uprooted trees near Turgo. This calculation results in significantly lower dynamic pressures, ~400–700 Pa, required to uproot the trees.

7.2.2. Broken bamboo and upright tree

At another point near Turgo, the surge broke hollow

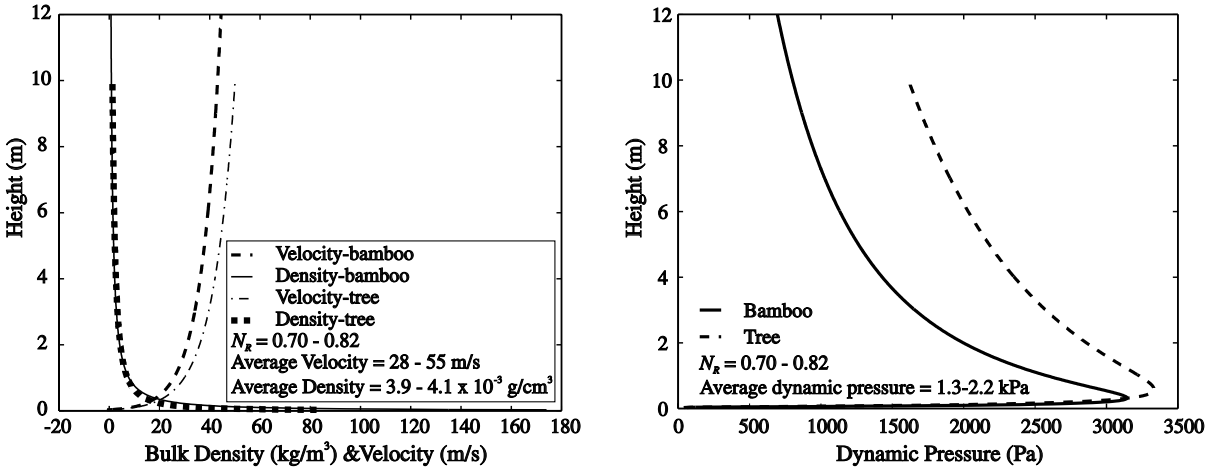

Fig. 5. Calculated current density, velocity, and dynamic pressure profiles using ruptured bamboo and unbroken tree near Turgo village, Merapi volcano, Parameters: $h_c = 50\ m$, $\rho_{avg} = 1.2 \times 10^{-3}$ g/cm^3 ($C_{avg} = 4.6 \times 10^{-4}$), $N_R = 0.72 - 0.80$, $U^* = 2.6$ m/s.

stalks of bamboo ($h = 12$ m; $r = 7.5$ cm), but failed to rupture a neighboring delimbed tree of similar dimensions ($h = 10$ m; $r = 7.5$ cm). Therefore the induced stress surpassed the rupture stress of bamboo, but did not reach the rupture stress of the tree trunk.

For the bamboo we used $r_o = 7.5$ cm, $r_i = 6.5$ cm and $\sigma_{ult} = 84$ MPa (Janssen, 1980). Using Eqs. (8b) and (27), $P_{dyn} = 1.0$ kPa in order to rupture the stalks of bamboo, and $P_{dyn} = 2.0$ kPa in order to rupture the tree. For this calculation, in the absence of better data, we used the rupture strength of Douglas fir for the tree.

Using 5 cm deposit thickness, surge height of 50 m, an air density of 0.74×10^{-3} g/cm^3 at 200°C, and the methods of Section 4, the maximum average surge current density near Turgo was $1.2\ (\pm 0.5) \times 10^{-3}$ g/cm^3 ($C_{avg} = 4.6 \times 10^{-4}$). Uncertainty results from ±20% variations in deposit thickness and ±20% variations in cloud height. Using the methods employed in Section 6.1.2, convergence for rupture of the bamboo occurs at $N_R = 0.82$, where $C_o = 5.5 \times 10^{-3}$, $U^* = 2.6$ m/s, $V_{ho} = 37(\pm 9)$ m/s, $\rho_{ho} = 3.9 \times 10^{-3}$ g/cm^3 and $P_{dyn} = 1.3$ kPa. The P_{dyn} necessary for rupturing the tree is 2.2 kPa, converging at $N_R = 0.70$ with $U^* = 3.7$ m/s, $V_{ho} = 45(\pm 10)$ m/s and $\rho_{ho} = 4.1 \times 10^{-3}$ g/cm^3 ($C_{ho} = 16 \times 10^{-4}$).

Therefore, our analysis constrains the velocity of the ash-cloud surge on November 22, 1994 at this location from 28 m/s (the lower limit of uncertainty required to rupture the bamboo) to 55 m/s (the upper limit required to rupture the tree). However, we are aware that the damage of the tree and the bamboo could also be explained by small-scale spatial velocity variations within the turbulent boundary layer of the surge. Fig. 5 shows the estimated vertical velocity, density, and dynamic pressure profiles for the surge near Turgo. Notice that, unlike the solution in Fig. 3, the dynamic pressure varies greatly with h, with a large peak occurring just below 0.5 m above the surface. This is because this calculation converges at $N_R = 0.70 - 0.82$, substantially higher than the $N_R = 0.27$, presented in Fig. 3. As shown in Fig. 2, the density profile approaches uniform distribution as N_R approaches zero.

Theoretical estimates using a first order velocity reconstruction using the approximate two-parameter dynamic model of Perla et al. (1980) suggest that the velocity range near Turgo for this event may have been about 25–50 m/s (Fig. 6). Kelfoun et al. (2000 – this volume) have suggested a similar result.

We recognize that the methods of Section 4, which we use to determine maximum average current density ρ_{avg}, require a significant assumption, namely that all material deposited downstream of the failed object was suspended in the current over the specified horizontal distance at the same time. Therefore, for this example case, we test the sensitivity of the final

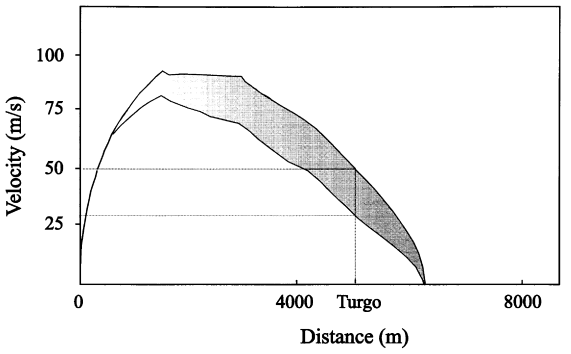

Fig. 6. Approximate velocity–distance plot for ash-cloud surge at Merapi volcano, for November 22, 1994 event. Plot based on Perla et al. (1980) model using friction coefficients from 0.14 to 0.2, and mass/density ratios range 3.33–3.7. Corresponding event durations range from 182 to 123 s. The topographic profile is drawn from the lava dome through Tritis village, west of Turgo. Shaded region represents approximate feasible velocity range based on upper and lower limits of assumed parameters. Dotted lines indicate range of values calculated for Turgo village. The location of Turgo is noted.

velocity estimate, V_{ho}, to maximum average cloud density, ρ_{avg}. Again, using the methods initially described in Section 6.1.2, we calculate the current velocity V_{ho} just sufficient to rupture the bamboo near Turgo village for a wide range of average current densities, ρ_{avg}. For ρ_{avg} from 0.50 to 3.0×10^{-3} g/cm^3, the estimated velocity required to rupture the bamboo varies from 75 to 20 m/s. A 71% variation in average current density, ρ_{avg}, results in a 37% variation in estimated current velocity over the height of the failed object, V_{ho}.

8. Discussion

Table 2 summarizes for all cases the input parameters and results, compares estimated dynamic pressure from the two methods illustrated in the text, and compares calculated values with other estimates.

In all of our test cases, the simplified *vertically uniform* (Section 6.1.1) and the *vertically non-uniform* (Section 6.1.2) methods of determining minimum dynamic pressure produced similar results. When modeling vertical density and velocity variations, we found it necessary to determine corresponding values of shear velocity and distribution Rouse number using an iterative method. This allowed us to estimate near-ground current density, velocity, and dynamic pressure profiles, given our assumed profile models. The *vertically non-uniform* treatment of examples at Unzen, Higaturu and Merapi indicate that average current densities over the height of the failed objects (for sizes 10–15 m) are approximately 2–5 times that of the estimated maximum current average density. This factor is close to that of snow avalanche near-ground density magnification (2–4 ×) indicated by laboratory experiments (Hopfinger and Tochon-Danguy, 1977). Therefore a simple and reasonable estimate of minimum dynamic pressure, P_{dyn}, may be made by the *vertically uniform* (Section 6.1.1; Eqs. (8) and (22)) method, and a simple near-ground velocity estimate can be made by assuming this density magnification. Note, however, that the near-ground density magnification for the Mount St. Helen's calculations (~8 ×) did not fall within the same range as those of the other example cases.

Also, measured velocity values, if available, can be used to estimate near-ground current bulk densities, as shown above for the "reversed" calculations.

Again, our whole-current average density estimates are maxima because we assume that all material deposited between the failed object and the end of the deposit was suspended in the current over this horizontal distance during a single instant. This results in corresponding minimum velocity estimates. In our analysis, the density of the current over the height of the failed object was determined using the relationship of Valentine (1987). A logarithmic velocity profile was assumed using a general relationship for turbulent flow over a rough surface. In most cases this method seemed to provide a reasonable velocity estimate, verified to a first approximation by using current velocities estimated from other procedures. However, we recognize that the convergent Rouse number, and the resulting velocity and density profiles, are valid for a current dynamic pressure exactly sufficient to cause the failure of the object. Thus, the solution is non-unique. The convergent velocity is moderately dependent upon the grain-size distribution used to determine the distribution Rouse number, with a variation of ±3 m/s for a wide range of surge deposit distributions.

The utility poles ruptured by the 1991 Unzen

Table 2
Summary of results. Dynamic pressure, velocity and current bulk density results are averages over the height of the failed object. Values of dynamic pressure estimated assuming *vertically uniform*, and *vertically non-uniform* assumptions are compared

Location and event	Failure type	Dynamic pressure (kPa) (*vertically-uniform*)	Dynamic pressure (kPa) (*vertically non-uniform*)	Velocity (m/s)	Bulk density ($\times 10^{-3}$ g/cm^3)	Independent dynamic pressure estimates (kPa)	Independent velocity estimates (m/s)
Mt. Unzen June 1991	Ruptured utility pole	8.0	7.4	58–78	3.4 ($C_{ho} = 13 \times 10^{-4}$)		26–28 Doppler radar (Nakada and Fujii, 1993) 60–100 energy line (Yamamoto et al., 1993)
	Uprooted tree	1.9		27–37	4.4 ($C_{ho} = 17 \times 10^{-4}$)		
Mt. St. Helens May, 1980	Ruptured Douglas Fir	39.7	43	110–130	8.3 ($C_{ho} = 32 \times 10^{-4}$)		120–140 (Moore and Rice, 1984)
Mt. Lamington 1951	Bent hollow flagpole:	1.3–2.1	1.5–2.2	29–38	4.3–4.7 ($C_{ho} = 17 - 18 \times 10^{-4}$)	7–20 (Valentine, 1998)	98 (assuming air ρ) (Hool, 1958) 27–93 (Taylor, 1958)
		1.3–24					
Merapi Volcano Turgo Village 22 Nov 94	Uprooted tree	0.4–1.9				2–20 based on Valentine (1998)	25–50 (Kelfoun et al., 1999); modeling by Perla method (This volume)
	Broken bamboo	1.0	1.3	28–55	4.1 ($C_{ho} = 16 \times 10^{-4}$)		
	Preserved teak	2.0	2.2		3.9 ($C_{ho} = 15 \times 10^{-4}$)		

ash-cloud surge offer the test case with the fewest complications. The utility poles are uniform cylinders with strengths that should fall close to standard lumber strengths. The most important parameters to constrain are the dimensions of the pole, pole strength, cloud height, deposit thickness and grain-size distribution.

Some assumptions for determining the dynamic pressure necessary to cause damage to live trees include the following: ultimate strengths for lumber and live trees have been assumed to be similar; uprooting-test data for trees of small diameter have been extrapolated to trees and root-systems of larger size; and the trees have been delimbed before being toppled, providing justification for modeling them as cylinders. In the examples cited, these assumptions seem reasonable to a first approximation. Trees with some limbs remaining during blow-down can be treated in a different manner.

The case of the bent flagpole at Lamington offers an opportunity to constrain both lower limit and upper limit current properties. Our analysis of the pole suggests dynamic pressures of 1.3–24 kPa at Higaturu, bracketing Valentine's (1998) estimate of 7–20 kPa based on equivalent damage of houses compared to the effects of nuclear weapons. The calculations suggest that the damage occurred progressively over time, commencing with dynamic pressures in excess of 1.3 kPa but not more than 2.8 kPa, and later reaching as high as 24 kPa. These results, however, are dependent upon the accuracy of strength characteristics of the pole, particularly the level of strain hardening and joint properties and upon the assumed sequence of events.

For the case of Turgo Village at Merapi volcano, our results suggest dynamic pressures of 2–4 kPa and velocities of 28–55 m/s. This result is consistent with approximate flow model calculations based on run out, event duration, and simplified flow parameters. Concrete homes in Turgo Village underwent no structural damage but many peaked tile roofs were damaged and windows were blown out. Comparison to damage from nuclear weapons blasts suggests that the dynamic pressure reached or exceeded 2–4 kPa in order to destroy windows, but did not exceed 10–20 kPa, the range at which complete failure of well constructed roofs is likely (Valentine, 1998).

After calculating current particle concentrations, densities and velocities, it is possible to compute the Reynolds Number, *Re*, of the currents in order to validate our assumed C_D. For the calculated velocities, and bulk viscosities determined for a dusty gas (Wohletz, 1998), corresponding values of *Re* ranged from from 4.5×10^3 to 2.3×10^5, where the Mount St. Helens current is the upper-bound value. Within this range, assuming $C_D = 1.1$ is reasonable for an individual tree.

However, it is important to recognize that the spatial variation of velocity in a turbulent surge can be significant, even over a small distance. This variation might in some cases explain such observations as the ruptured bamboo and the adjacent preserved tree near Turgo village. Further, the treatment of individual trees greatly simplifies the dynamics of strong gusts or pyroclastic currents acting on a forest. Our treatment ignores the possibility of large flying debris hitting the trees used in our analyses, causing them to fail. Also, it has been noticed in wind tunnel tests of 'forests,' that wind striking the front edge of a forest "rises sharply upwards, becomes turbulent and strikes downwards some way into the forest, creating violent oscillating forces on the trees" (Allen, 1982; pp. 74–75), indicating that our treatment cannot account for all the complexities potentially offered by such systems.

9. Conclusions

The cases examined above suggest that the simple method of this paper yield good first-order estimates of current dynamic pressure, and in some cases velocity and/or density. The calculated results correlate reasonably well with observations and independent theoretical calculations. Dynamic pressure is a parameter that could be plotted on maps, and when data permit, "contoured" to indicate the variations in dynamic properties of pyroclastic currents.

Other refinements of this method are feasible, and we emphasize that the approach can be adapted to any object of different shape and drag coefficient.

Important parameters include object strength, object dimensions, degree of delimbing, degree of trunk taper, qualitative nature of the rupture, total deposit thickness, grain-size characteristics of deposits, and cloud height.

Acknowledgements

Parts of this work were supported by the US Geological Survey USAID VCAT mission to Merapi volcano in 1995, and NSF grants EAR 93-16739, 96-14622 and 96-28413 to B.V. The assistance of Dr. Mas Atje Purbawinata and the staff of Merapi Volcano Observatory is greatly appreciated. We are likewise grateful to Ron Kopstead of the U.S. Forest Service and Ross Gilchrist of Weyerhaeuser for much assistance. The paper was improved as a result of reviews by G. Valentine, R. Denlinger, James Ewart, and one anonymous reviewer.

References

Abdurachman, E.K., Bourdier, J.L., Voight, B., 2000. Nuées ardentes of 22 November 1994 at Merapi volcano, Indonesia. J. Volcanol. Geotherm. Res. 100, 345–361.

Allen, J.E., 1982. Aerodynamics, Granada, New York, 534 pp.

Allen, J.R.L., 1970. Physical Processes of Sedimentation. Elsevier, New York, 248 pp.

Anderson, J.D., 1991. Fundamentals of Aerodynamics. McGraw-Hill, New York, 772 pp.

Beer, F.P., Johnston, E.R., 1981. Mechanics of Materials. McGraw-Hill, New York, 616 pp.

Clarke, A.B., Hidayat, D., Voight, B., 1997. Pyroclastic current speedometer/densitometer from dynamics of tree or pole blow-down. Abstr. IAVCEI General Assembly: Volcanic Activity and the Environment, p. 8.

Druitt, T.H., 1980. Emplacement of the 18 May lateral blast deposit ENE of Mount St. Helens Washington. Bull. Volcanol. 54, 554–572.

Dunning, R., 1958. Appendix 1: Reports on the bending of the Higaturu Flagpole. In: Taylor, G.A., (Ed.), The 1951 Eruption of Mount Lamington, Papua. Department of National Development, Bureau of Mineral Resources, Geology and Geophysics, Bulletin No. 38, 100 pp.

Freundt, A., Bursik, M.I., 1998. Pyroclastic flow transport mechanisms. In: Freundt, A., Rosi, M. (Eds.), From Magma to Tephra: Modelling Physical Processes of Explosive Volcanic Eruptions. Elsevier, Amsterdam, pp. 173–245.

Glasstone, S., Dolan, P.J., 1977. The effects of nuclear weapons. US Dept. of Defense and Dept. of Energy, 653 pp.

Hool, J.N., 1958. Appendix 1: Reports on the bending of the Higaturu Flagpole. In: Taylor, G.A., 1958. The 1951 eruption of Mount Lamington, Papua. Department of National Development, Bureau of Mineral Resources, Geology and Geophysics, Bulletin No. 38, 100 pp.

Incropera, F.P., De Witt, D.P., 1990. Fundamentals of Heat and Mass Transfer. Wiley, New York, 919 pp.

Hopfinger, E.J., Tochon-Danguy, J.C., 1977. A model study of powder snow avalanches. J. Glaciol. 19, 343–356.

Janssen, J., 1980. The mechanical properties of bamboo used in construction. In: Lessard, G., Chouinard, A., (Eds.), Bamboo Research in Asia: Proceedings of workshop held in Singapore 28–30 May 1980. International Development Research Center, Ottawa, pp. 173–188.

Kelfoun, K., Legros, F., Gourgaud, A., 2000. A statistical study of trees damaged by the November 22, 1994 eruption of Merapi volcano (Java, Indonesia): relationships between ash-cloud surges and block-and-ash flows. J. Volcanol. Geotherm. Res. 100, 379–393.

Kieffer, S.W., 1981. Fluid dynamics of the May 18 blast at Mount St. Helens. In: Lipman, P.W., Mullineaux, D.R. (Eds.), U.S. Geol. Surv. Prof. Pap. 1250, 379–400.

Kunii, D., Levenspiel, O., 1977. Fluidization Engineering. Wiley, New York, 534 pp.

Miyabuchi, Y., 1999. Deposits associated with the 1990–1995 eruption of Unzen volcano Japan. J. Volcanol. Geotherm. Res. 89, 139–158.

Moore, J.G., Rice, C.J., 1984. Chronology and Character of the May 18, 1980, Explosive Eruptions of Mount St. Helens. In: Explosive Volcanism: Inception, Evolution and Hazards, National Academy Press, Washington, DC, pp. 133–142.

Moore, J.G., Sisson, T.W., 1981. Deposits and effects of the May 18 pyroclastic surge. In: Lipman, P.W., Mullineaux, D.R. (Eds.), U.S. Geol. Surv. Prof. Pap. 1250, 421–438.

Nakada, S., Fujii, T., 1993. Preliminary report on the activity at Unzen Volcano (Japan), November 1990–November 1991: Dacite lava domes and pyroclastic flows. J. Volcanol. Geotherm. Res. 54, 319–333.

Panton, R.L., 1996. Incompressible Flow. Wiley, New York, 837 pp.

Perla, R., Cheng, T.T., McClung, D.M., 1980. A two-parameter model of snow avalanche motion. J. Glaciol. 26 (94), 197–207.

Popov, E.P., 1952. Mechanics of Materials, Prentice Hall, Englewood Cliffs, NJ, 441 pp.

Rae, W.H., Pope, A., 1984. Low-Speed Wind Tunnel Testing. Wiley, New York, 534 pp.

Snellgrove, T.A., Kendall-Snell, J.A., Max, T.A., 1983. Damage to national forest timber on Mount St. Helens. J. Forestry 81, 368–371.

Sparks, R.S.J., Wilson, L., Hulme, G., 1978. Theoretical modelling of the generation, movement, and emplacement of pyroclastic flows by column collapse. J. Geophys. Res. 83 (B4), 1727–1887.

Terzaghi, K., Peck, R., 1948. Soil Mechanics in Engineering Practice. Wiley, New York, 543 pp.

Taylor, G.A., 1958. The 1951 eruption of Mount Lamington, Papua. Department of National Development, Bureau of Mineral Resources, Geology and Geophysics, Bulletin No. 38, 100 pp.

Valentine, G.A., 1987. Stratified flow in pyroclastic surges. Bull. Volcanol. 49, 616–630.

Valentine, G.A., 1998. Damage to structures by pyroclastic flows and surges, inferred from nuclear weapons effects. J. Volcanol. Geotherm. Res. 87, 117–140.

Waitt, R.B., 1981. Devastating pyroclastic density flow and attendant air fall of May 18-stratigraphy and sedimentology of deposits. In: Lipman, P.W., Mullineaux, D.R. (Eds.) Geol. Surv. Prof. Pap. 1250, 439–458.

Wohletz, K.H., 1998. Pyroclastic surges and compressible two-phase flow. In: Freundt, A., Rosi, M. (Eds.), From Magma to Tephra: Modelling Physical Proocesses of Explosive Volcanic Eruptions. Elsevier, Amsterdam, pp. 247–312.

Wohletz, K.H., Sheridan, M.F., 1979. A model of pyroclastic surge. Geol. Soc. Am. Spec. Pap. 180, 177–193.

Yamada, T., Yajima, S., 1992. A study on the pyroclastic flows and debris flows associated with the Mount Unzen eruption in 1991. Technical Memorandum of PWRI No. 3141, 39 pp.

Yamamoto, T., Takarada, S., Suto, S., 1993. Pyroclastic flows from the eruption of Unzen Volcano, Japan. Bull. Volcanol. 55, 166–175.